Version of Record: https://www.sciencedirect.com/science/article/pii/S0022169421014372
Manuscript_f47d56753ad2e147092814dfffb1b39d

Last two millennia of streamflow variability in the headwater catchment of the Yellow River basin reconstructed from tree rings

Wenzhuo Wang[1], Zengchuan Dong[1*], Mukund Palat Rao[2,3,4], Upmanu Lall[5,6], Benyou Jia[7]

[1] College of Water Resources and Hydrology, Hohai University, Nanjing 210098, China.
[2] Cooperative Programs for the Advancement of Earth Science, University Corporation for Atmospheric Research, Boulder, CO 80307, USA

[3] Tree Ring Laboratory, Lamont-Doherty Earth Observatory of Columbia University, Palisades, NY 10964, USA

[4] Department of Plant Science, University of California Davis, Davis, CA 95616, USA

[5] Columbia Water Center, Columbia University, New York, NY 10027, USA

[6] Department of Earth and Environmental Engineering, Columbia University, New York, NY 10027, USA

[7] Nanjing Hydraulic Research Institute, Nanjing 210029, China.

Corresponding author: Zengchuan Dong, College of Water Resources and Hydrology, Hohai University, Nanjing 210098, China (zcdong@hhu.edu.cn)

Highlights:

- A new annual (Nov-Oct) streamflow reconstruction of HCYRB at Tangnaihai Station of nearly two millennia was presented
- The nested principal component regression model is improved by the stepwise best tree-ring subset selection method in terms of AIC, $CRSQ$, $VRSQ$, CE, and RE
- The significant high-flow periods of HCYRB are the early 3rd century, circa 300 C.E., early 13th century, 16th century and circa 1900 C.E., while the low-flow periods are the late 5th century and late 15th century
- The reconstruction suggests that a warm climate is more likely accompanied by a high-flow period and low-flow periods are more likely to happen in cold periods associated with the Asian Summer Monsoon and solar activity
- The results provide adequate data foundation to analyze characteristics of streamflow of HCYRB and long-term optimal operation of Longyangxia over-year regulation reservoir

Abstract

The headwater catchment of the Yellow River Basin (HCYRB) controls 35% of the streamflow of the Yellow River (YR) which faces increasing water shortages. To better understand streamflow variability in the region we require a better understanding of high and low flow characteristics. This study presents a new annual (Nov-Oct) streamflow reconstruction at the Tangnaihai station in the HCYRB for the last two millennia (159-2016 C.E.) using 12 tree-ring chronologies. The nested principal component regression model combined with the stepwise best subset selection method was proposed to improve the temporal length and model skill of reconstruction. The stepwise best subset selection method was presented to select the best principal components subset, instead of a confidence test, based on k-fold cross-validation error and Akaike's information criteria (AIC). The model assessment results verify that the proposed model exhibits strong reconstruction skills. Besides, the magnitude and duration of both high and low flow periods were analyzed. The results show that (1) the significant high-flow periods are the early 3rd century, circa 300 C.E., early 13th century, 16th century and circa 1900 C.E., while the low-flow periods are the late 5th century and late 15th century; (2) the durations and magnitudes of low-flow periods are longer and larger than high-flow periods and the severities of high-flow periods are greater than low-flow periods. The reconstruction also suggests that a warm climate is more likely accompanied by a high-flow period and low-flow periods are more likely to occur in cold periods associated with the Asian Summer Monsoon and solar activity.

Keyword: annual streamflow reconstruction; stepwise best subset selection method; tree ring; the Yellow River Basin

1 Introduction

The Yellow River (or Huang He) is the second-longest river in China and the sixth-longest river in the world (Huang et al., 2015). With a length of 5464 km and a drainage area of 795 thousand km^2, the river, stretches eastward over 9 provinces through the arid and semi-arid regions of northern China (Shiau et al., 2007). The Yellow River plays an important role in many aspects of the country, the 9 provinces along which are responsible for one third of national grain production of 0.23 billion tons and 25% of national GDP of 24741 billion yuan in 2019. The utilization of the Yellow River is therefore of key importance for the sustainable economic and social development of China.

However, the Yellow River basin has suffered serious problems of water shortage and uneven distribution both temporally and spatially (Wang et al., 2018a). Looking back through history, the Yellow River basin experienced 1,070 recorded annual droughts from 1766 B.C. to 1944 C.E. In the past 40 years, severe droughts continually occurred in the upper and middle reaches, causing a significant reduction in grain production. The drought in 1980 reduced a grain production of 3.32 million tons. The drought in 1982 destroyed 10 million mu (670 thousand ha) of cultivated land. The disaster in 1994 reached 60 million mu (4 million ha) and the grain production decreased 6 million tons. The drought in 1997 not only caused declines of many crops but also led to the drying up of the river for 227 days. Since 2000, droughts even occurred more frequently. For example, from the winter of 2008 to the spring of 2009, most of the major wheat-producing provinces in northern China suffered from drought with a drought area of 113 million mu(7.8 million ha). (Wang et al., 2016a)

One of the largest water supply regions in the Yellow River Basin is the headwater catchment (HCYRB), which refers to the area upstream of the Tangnaihai Station on the main Yellow River (Zhang et al., 2015). It has a mean elevation of 4000 m and is located in the northeastern Tibetan Plateau. The catchment covers a drainage area of 121,972 km^2, accounting for 16% of the total area of the Yellow River Basin, and controls a river section of 1,553 km, accounting for 28.4% of the length of the river(Wang et al., 2018b). The HCYRB produces 35% of the total streamflow in the Yellow River, so water yield variations in the basin seriously affect the water supply and economic development in the middle and lower reaches of the Yellow River(Zhang et al., 2014). An improved understanding of streamflow variability at HCYRB will, therefore, help to elucidate drought scenarios and efficiently determine water resources allocation strategies for the whole basin.

The short length of the observed streamflow record at HCYRB limits the understanding of its time-series characteristics, variability, and trend. Large-scale climate phenomena, which directly affect local weather and indirectly influence streamflow variability, often exhibit interdecadal and centennial timescales(Yin et al., 2021). For example, periodic climate phenomena such as Pacific Decadal Oscillation (PDO), Atlantic Multidecadal Oscillation (AMO), and North Atlantic Oscillation (NAO) exhibit one phase with 20-80 years. Streamflow driven by these climate indices should also exhibit interdecadal variabilities. However, short streamflow observations only cover one to two phases and thereby are not well suited to meet the data length requirement to analyze long-term statistic characteristics and the variability in discharge (Stockton and Jacoby, 1976; Woodhouse and Lukas, 2006). Therefore, longer records are required not only for a better understanding of the past high and low flows but also for the interdecadal variability driven by large climate indices in the long period (Timilsena et al., 2009).

Tree rings have been used to extend the record of streamflow since, in specific environments, their annual widths may be driven by the same climate as annual streamflow (Keyimu et al., 2020; Meko et al., 1995). The principal component regression is widely used in reconstruction based on multiple tree rings, which exhibits optimal model skill compared with simple regression by transforming the highly correlated tree rings into uncorrelated ones

(Fritts, 1991; Smith and Stockton, 1981). Some previous studies have already focused on the streamflow reconstruction of HCYRB using tree rings. Gou et al. (2007) and Gou et al. (2010) respectively reconstructed the streamflow of Tangnaihai Station for the past 593 years using principal component regression based on 6 *Juniperus Przewalski* tree-ring chronologies and for the past 1234 years using a regression-based on a *Juniperus Przewalski* tree-ring chronology. Several severe droughts in the late 15th century and low-flow periods in 1820-1830, 1480-1490 along with a decreasing trend in the modern instrumental period were recognized in both Gou et al. (2007) and Gou et al. (2010). The existing research laid a good foundation for the streamflow reconstruction of HCYRB using tree rings.

However, the employed tree rings are few and typically have varying lengths, limiting the temporal length of reconstructions. A new annual (Nov-Oct) streamflow reconstruction of HCYRB at Tangnaihai Station is presented, which not only spans a longer time coverage of nearly two millennia (between 159-2016 C.E.) but also demonstrates improved reconstruction skill compared to the older reconstructions. To realize this goal, the stepwise best tree-ring subset selection method is proposed into the nested principal component regression model and an improved tree-ring network based on a set of 12 tree-ring chronologies, which has become available recently, were used. The choice of the streamflow season from prior year Nov to current year Oct considers both the flood/non-flood season of the Yellow River Conservancy Commission of the Ministry of Water Resources and growing season of tree rings(Li et al., 2016; Zhang et al., 2019). This long-term extension of streamflow provides sufficient data to assess interannual and interdecadal variabilities and capture high-flow and low-flow periods of streamflow at HCYRB in history, which indicate the impacts of climate change and long-term evolution law including periods. It serves as a useful reference for long-term streamflow prediction and water resources planning and management in the Yellow River. The goals of this research include (1) presenting a new annual (Nov-Oct) streamflow reconstruction that is longer than the existing ones; (2) analyzing the high-flow and low-flow variabilities of streamflow at HCYRB in the nearly last two millennia.

2 Study area and data

2.1 The headwater catchment of the Yellow River basin

The HCYRB is located on the northeastern fringe of the Tibetan Plateau in western China (Gou et al., 2007). The annual temperature and precipitation in this region are affected by the Asian summer monsoon from the Bay of Bengal. Both temperature and precipitation increase from May to July varying from – 4 °C to 2 °C and 250 mm to 750 mm respectively (Zhang et al., 2014). Moreover, there is a significant difference in the spatial distribution of precipitation at the HCYRB, as the average annual precipitation in the northwest of HCYRB is only 200 mm, but may exceed 700 mm in the south-eastern part (Zheng et al., 2018).

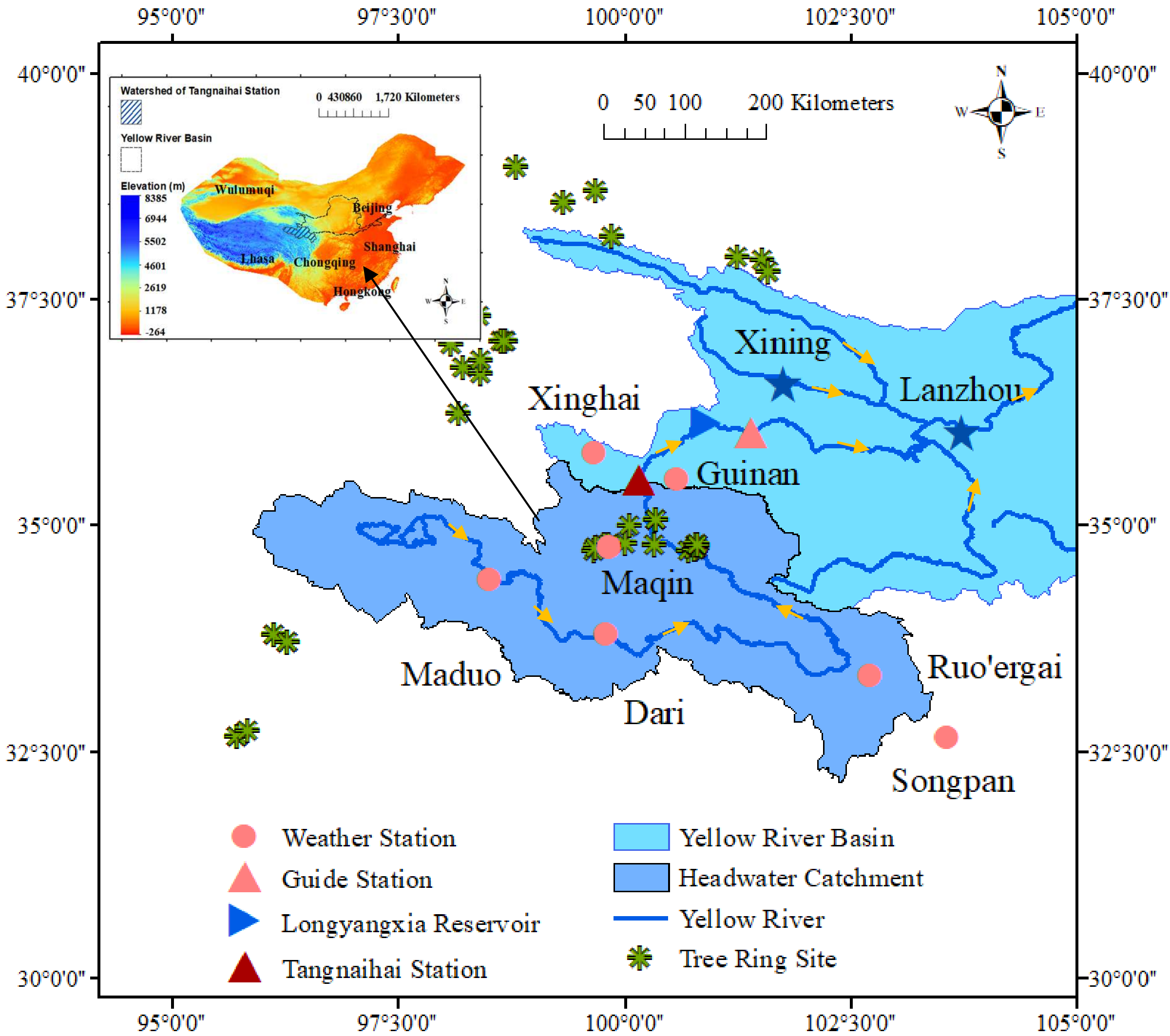

Figure 1 Locations of the Yellow River, Tangnaihai Station and the seven weather stations

Temperature and precipitation data of seven meteorological stations proximately located to the HCYRB between 1960 and 2016 were obtained from the National Meteorological Information Center of China （http://data.cma.cn）. The location network of the seven meteorological stations is shown in Figure 1. The seasonal distribution of mean temperature and precipitation of seven meteorological stations are shown in Figure 2 with a comparison of average monthly cumulative streamflow discharge between 1960 and 2016. The climatology of streamflow at the Tangnaihai hydrological station is similar to those of precipitation and temperature. The peak flow season between April-October coincides with increased temperature and warmer conditions and conversely, the November-March dry season is coincident with low precipitation and cool temperatures.

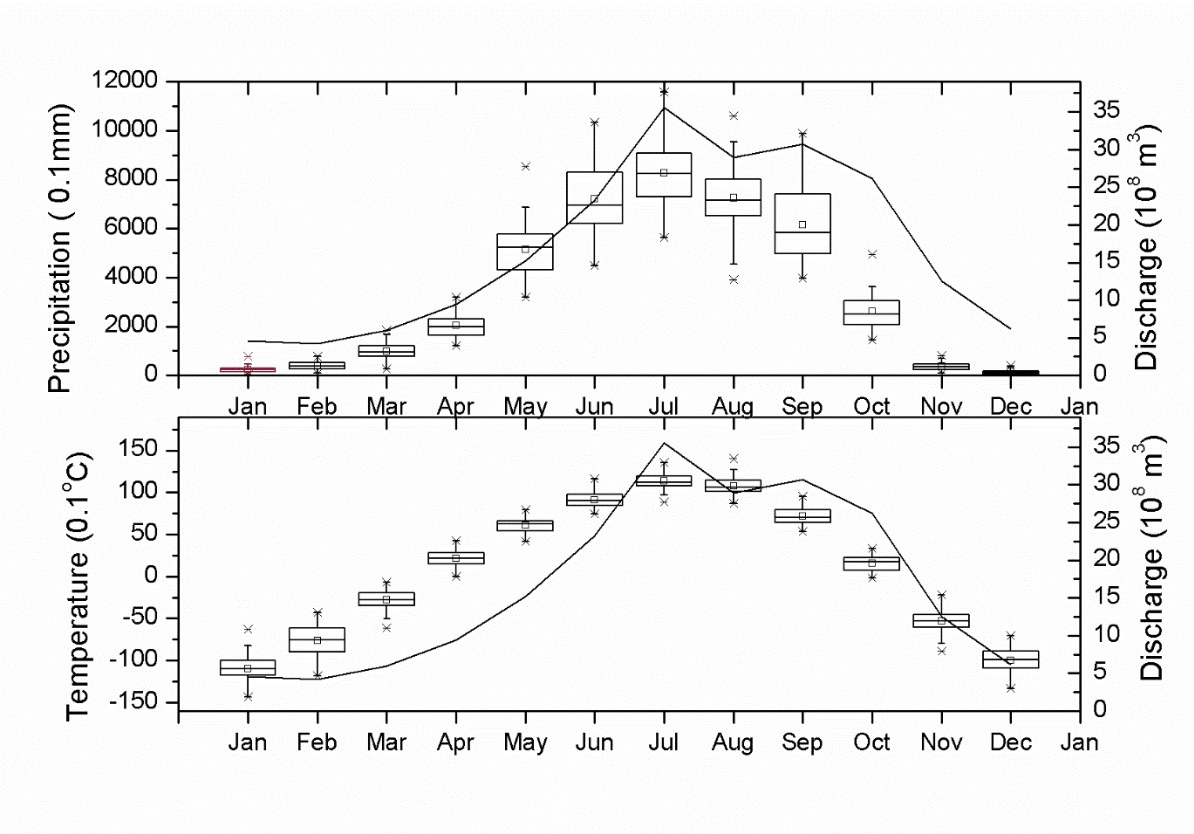

Figure 2. Monthly precipitation and monthly mean temperature boxplots of seven meteorological stations between 1960 and 2016 at HCYRB

2.2 The headwater catchment discharge of the Yellow River basin at Tangnaihai Station

The instrumental streamflow data used for reconstructing the discharge of HCYRB were obtained from the Yellow River Conservancy Commission of the Ministry of Water Resources (http://www.hydroshare.org/resource/bde8bcf096544ce7b183de784a378c52). The monthly streamflow record at the Tangnaihai Station, which serves as the outlet of the headwater catchment of the Yellow River Basin, spans 1956 to 2016 C.E. To increase the reliability of the reconstruction, the streamflow record of the station was extended to 1920 using instrumental data of Guide Station. It is located 189 km downstream of Tangnaihai Station, which can be considered to be consistent with Tangnaihai Station before the

Longyangxia Reservoir was built in 1976. The location network of Tangnaihai Station and Guide Station in the Yellow River Basin is shown in Figure 1. Therefore, the specific streamflow records used in this paper were:

(a): unimpaired monthly streamflow of Tangnaihai Station (100°9′ E, 35°3′ N) between 1956-2016

(b): unimpaired monthly streamflow of Guide Station (101°24′ E, 36°2′ N) between 1920-1976

The annual streamflows at Tangnaihai Station and Guide Station are shown in Figure 3. There is a significant association between the streamflows of the two stations with a Pearson correlation of 0.9985 (21 years). Figure 3 demonstrates that the annual streamflow of Guide Station matches Tangnaihai Station well for the years of overlap before Longyangxia Station was built (1956-1976).

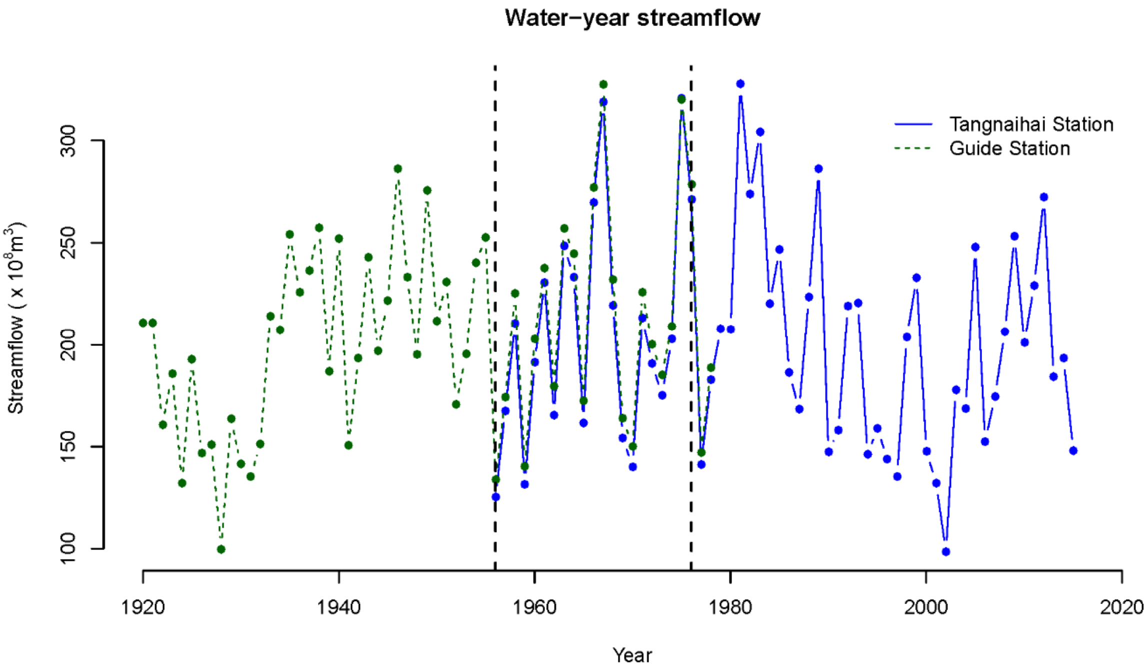

Figure 3 Annual (previous Nov to Oct) streamflow variabilities of Tangnaihai Station and Guide Station

2.3 Tree-ring chronologies

Considering climate factors are not limited to hydrological basins, all tree-ring chronologies in or near HCYRB, where may share a similar climate to HCYRB, served as potentially useful tree-ring candidates to reconstruct discharge at Tangnaihai Station. The raw ring width data, which had been cross-dated and evaluated using the COFECHA program, were downloaded from the International Tree-Ring Data Bank (ITRDB) (https://www.ncdc.noaa.gov/data-access/paleoclimatology-data/datasets/tree-ring) (Ahmed et al., 2013; Cook et al., 2013; Emile-Geay et al., 2017). 49 tree-ring chronologies were obtained and the map of the tree-ring networks is shown in Figure 1.

First, standardization of tree rings was conducted to maximize the elimination of the non-climatic variability, including the non-stationary feature and heteroscedasticity, and preserving the low-frequency variability in the tree-ring series (Cook, 1985; Fritts, 1976; Helama et al., 2004). In this study, the raw ring width data for each site were standardized using the signal-free method in combination with a negative exponential curve or an age-dependent smoothing spline to preserve the maximum amount of common low to medium frequency variability in the tree-ring data (see detail in Melvin and Briffa (2008)and Melvin et al. (2007)). The standard chronologies, rather than residual chronologies, were used because they include autoregressive persistence likely due to climate.

Next, the processes of prescreening and screening of the standard tree-ring chronologies were carried out to select appropriate tree-ring chronologies as predictors. The chronologies were first prescreened, such that only series that had an end-year in or later than 2001 was retained. 79 chronologies meet the length requirement considering the one-year lag.

Then, correlation analysis was implemented to the pre-screened tree rings with the instrumental annual streamflow over the overlap period (1921-2001) for the screening. The tree-ring chronologies which were significantly (α=0.05) correlated with streamflow were chosen using a two-sided t-test. Finally, 12 screened tree-ring chronologies were retained for analysis. The general information is given in Table 1.

Table 1. General information about the selected chronologies

Site No.	Site Name	Location(°N, °E)	Start Year	End Year	Correlation	Lag
1	HAIYJP	(38.57,99.33)	368	2009	0.360	0
2	DULAJP	(36.23,98.17)	159	2011	0.290	0
3	MQCXJP	(35.07,100.35	1249	2001	0.310	0
4	MQFXJP	(34.75,99.68)	1230	2002	0.456	0
5	YYAHJP	(34.78,100.33)	1426	2002	0.450	0
6	TDCXJP	(35.07,100.35)	1130	2002	0.409	1
7	DLH1	(37.47, 97.23)	843	2001	0.460	0
8	DLH2	(37.47,97.22)	828	2001	0.383	0
9	WL2	(37.03,98.67)	845	2001	0.267	0
10	WL4	(36.68,98.42)	900	2001	0.347	0
11	WL1	(37.03,98.63)	856	2002	0.347	1
12	QML	(33.8,96.13)	1480	2002	0.440	0

3 Methods

Nested reconstruction models combining the principal component regression method and stepwise tree ring subset selection method were utilized to reconstruct annual (Nov-Oct) streamflow at HCYRB based on the selected tree-ring chronologies. The workflow of the proposed model is shown in Figure 1.

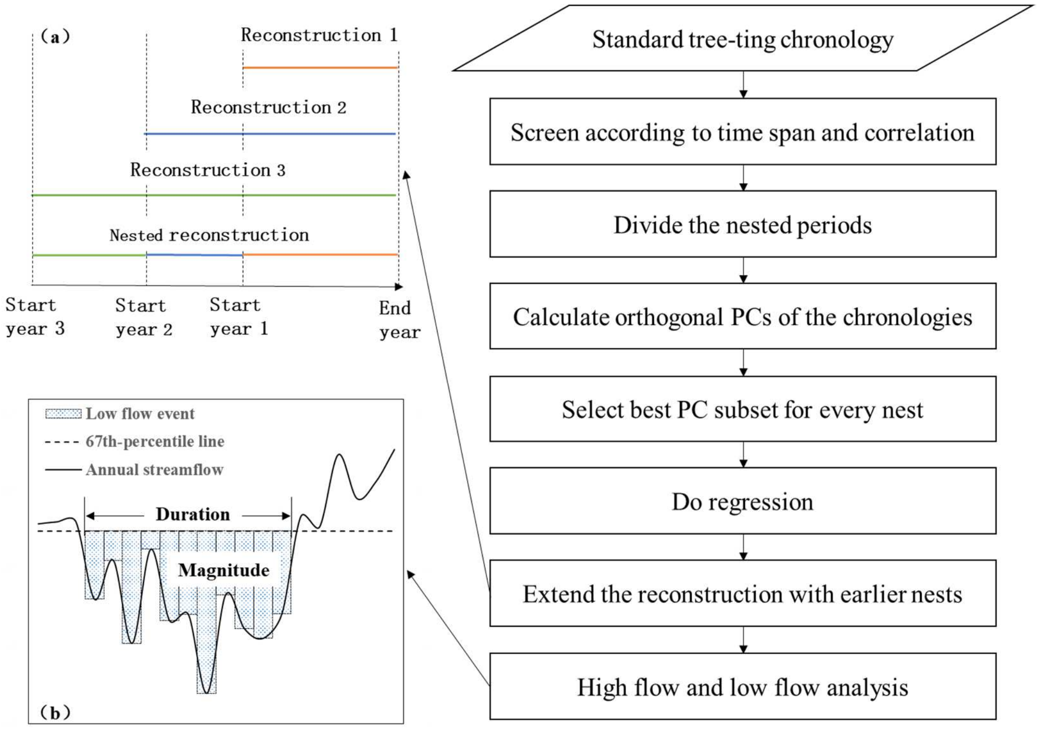

Figure 4. The workflow of the proposed nested principal component regression model combined with stepwise best subset selection method and evolution analysis

3.1 Nested principal component regression model

The nested principal component regression model extends streamflows using principal component regression over nested periods to produce the longest possible reconstruction from the available tree-ring data. The nested periods, which are separated by the start years of tree-ring chronologies, exhibit a multiple span structure with increasing start years and a common end year as (a) in Figure 4. Every nest requires vectors of the same length, but that the tree-ring predictors are all different lengths depending on how old the trees were. Because of this, nests have to be divided whenever the shortest chronology is dropped out of the dataset. To that end, we defined the difference between the start years of two spans of at least 30 years to avoid a large number of nests. In the nested model, the more recent nest of the reconstruction is usually more reliable than the earlier one because more tree-ring chronologies are involved (Meko et al., 2001). Therefore, the full nested reconstruction is then created by appending each subset-reconstruction extension back in time to the beginning of pre-existing shorter reconstruction (Cook et al., 2013).

Each reconstruction model extends streamflow using the principal component regression (PCR) approach based on the selected combination of tree-ring chronologies. In PCR, the principal component analysis was used first to transform the original predictors into a new set of independent principal components (PCs) by applying singular value decomposition to the covariance matrix of the selected chronologies (Meko et al., 2007). The PCs used in reconstruction were selected using stepwise best subset selection. Then, the log-linear regression function was utilized secondly to reconstruct streamflow based on the selected PC. The log-linear regression is capable of transforming the positively skewed streamflow data to a distribution that is closer to that of the chronologies (Margolis et al., 2011).

Before the PCR in each nest, the appropriate normalization is done to the ensemble of tree-ring chronologies with the mean and standard deviation of the calibration period. The normalization can be defined as

$$x_i^* = \frac{x_i - u_c}{\sigma_c} \quad (1)$$

where x_i is the original single tree-ring chronology; x_i^* is the normalized single tree-ring chronology; u_c and σ_c respectively represent the calibration period mean and standard deviation of original tree-ring chronologies.

After the PCR in each nest, the standard deviation of reconstructed streamflow in every nest is rescaled to observed records of the calibration period to recover lost variance. Rescaling can be defined as

$$Q_{i,j}^{*} = \left(\frac{Q_{i,j} - u_j}{\sigma_j} \right) \sigma + u_j \tag{2}$$

where $Q_{i,j}$ and $Q_{i,j}^{*}$ respectively denote the original and rescaled reconstructed streamflow in the nest j; u_j and σ_j respectively represent the calibration period mean and standard deviation of the original reconstructed streamflow in the nest j; σ is the standard deviation of instrumental streamflow.

These procedures are capable of avoiding the artificial variability in the extension using reconstructions in latter nests due to variance differences in regressions of different nests (Cook et al., 1994). The recovery of lost variance due to regression also provides for less biased comparisons of current with past, at the expense of increased uncertainty bounds in the reconstruction (Ammann et al., 2010).

3.2 The stepwise best subset selection method

The traditional significance test does not guarantee a great or stable model skill. The forward best subset selection method was implemented to choose the best principal component subset before the regression in each nest using the data of the calibration period. The method first selects different best models in different dimensions (the number of selected principal components) using k-fold cross-validation. Then the best principal component subset is selected among the different best models by calculating their Akaike's information criteria (AIC) values to avoid over-fitting. The subset with the lowest value was selected for both cross-validation error and AIC. The idea behind the best subset selection method is to select the principal component group with the lowest AIC instead of the traditional significance test. The k-fold cross-validation error in the best subset selection method is calculated as

$$\mathrm{CV}_k = \frac{1}{k}\sum_{i=1}^{k} RSS_k \tag{3}$$

where RSS_k is the residual sum of squares of the k-fold data. Here the 5-fold cross-validation was used.

The common calculation of the AIC algorithm is given by Schwarz (1978). For the linear regression with normal errors, AIC can be expressed as (Burnham and Anderson, 2004):

$$AIC = n\log\left(RSS / n\right) + 2V \tag{4}$$

where RSS is the residual sum of squares of the whole training data; V is the total number of parameters in the regression.

To simplify the process to avoid testing all possible combinations, the best subset was found by a stepwise procedure from the low dimension to high dimension: AIC was calculated after the subset selection in every dimension. The steps were driven by continuously increasing the dimension until the minimum AIC for the higher dimension was larger than the AIC of the previous one. The previous best subset in the lower dimension was selected as the final best subset. Though the selected principal component combination may not ensure the global optimum among all possibilities, it gives a more parsimonious model since it performs better than the model using all the variables (Hidalgo et al., 2000).

3.3 Streamflow reconstruction performance indicators

The observed streamflow records are partitioned into a model calibration period (1943-2002) and a validation period (1921-1942) to assess model performance. The parameters and optimal tree-ring subset are estimated and selected over the calibration period, while the model skill is assessed over the years of validation which gives a less biased performance estimate (Michaelsen, 1987).

To assess the skill of the nested reconstruction models, a set of calibration and validation statistics is implemented for every subset model. The widely-used performance indicators include calibration period coefficient of multiple determination ($CRSQ$), validation period square of the Pearson correlation coefficient ($VRSQ$), validation period reduction of error (RE), validation period coefficient of efficiency (CE), which work to detect the difference between the observed and reconstructed streamflow (Cook et al., 2013; Gaire et al., 2017; Rao et al., 2018). When they are positive, the estimated data contains more useful information than the mean value in the corresponding period, and vice versa (Devineni et al., 2013). Besides, they are proportional to the skill, which means the higher values the indicator values exhibit, the more accurate the estimated data is, and thereby the better performance the model shows.

3.4 High and low flow elucidation

High flow periods were identified as the year when the cumulative streamflow at least two years is the above 33rd percentiles of long-term streamflow, while low flow periods were identified as the year when the cumulative streamflow at least two years is the below 67th percentiles of long-term streamflow. To detect the temporal characters, the high (low) flow periods were analyzed in terms of the magnitude (total excess/deficit), the duration (years) and severity, and the frequency (see the detail in Timilsena et al. (2007)).

4 Results

In this section, the model assessment results are shown first. Then the reconstructed streamflow series is presented with anomalies and its statistical characteristics analyzed every ten decades. Finally, we explore the historical high and low flow periods and the teleconnection between the streamflow and large climate indices in HCYRB to provide information to streamflow prediction and long-term optimal operation of over-year regulation reservoirs, based on the reconstructed streamflow.

4.1 Model assessment

8 nested periods were divided according to the start years of the 12 tree-ring chronologies. The final reconstructed streamflow series was produced by extending the nested reconstructions. The 5-fold cross-validation errors and AIC values of the best subsets in different nests are also shown in table 2.

Table 2. Calibration/validation results of nested models. NTR is the number of tree-ring chronologies, while NPC is the number of selected PCs.

Nest	NTR	NPC	Start Year	CV of the best subset	AIC of the best subset
1	12	4	1480	17172.31	430.48
2	11	4	1385	16974.52	429.78
3	10	3	1249	18537.18	431.38
4	8	2	1130	22979.57	440.78
5	7	2	900	23425.70	443.89
6	6	2	857	23344.18	443.58
7	2	1	368	27412.72	450.83
8	1	1	159	26671.75331	450.70

Figure 5 shows the model skill assessment results including the AIC value. The values of $CRSQ$, $VRSQ$, CE and RE for almost all nests are positive, which are up to 0.37, 0.62, 0.57 and 0.69 respectively of the latest nest. Only the earliest nest of 159~368 C.E. shows poor performance in terms of CE, but all the other indicators give evidence of performance better than average. Consequently, the results indicate the higher accuracy of the reconstruction than the corresponding climatology on both the calibration period and validation period. Additionally, all of the $CRSQ$, $VRSQ$, CE, and RE variation lines of the proposed model are higher than the ones of the principal component regression method and the AIC line is lower, which give strong evidence of the more optimal model skill of the proposed model than he principal component regression method.

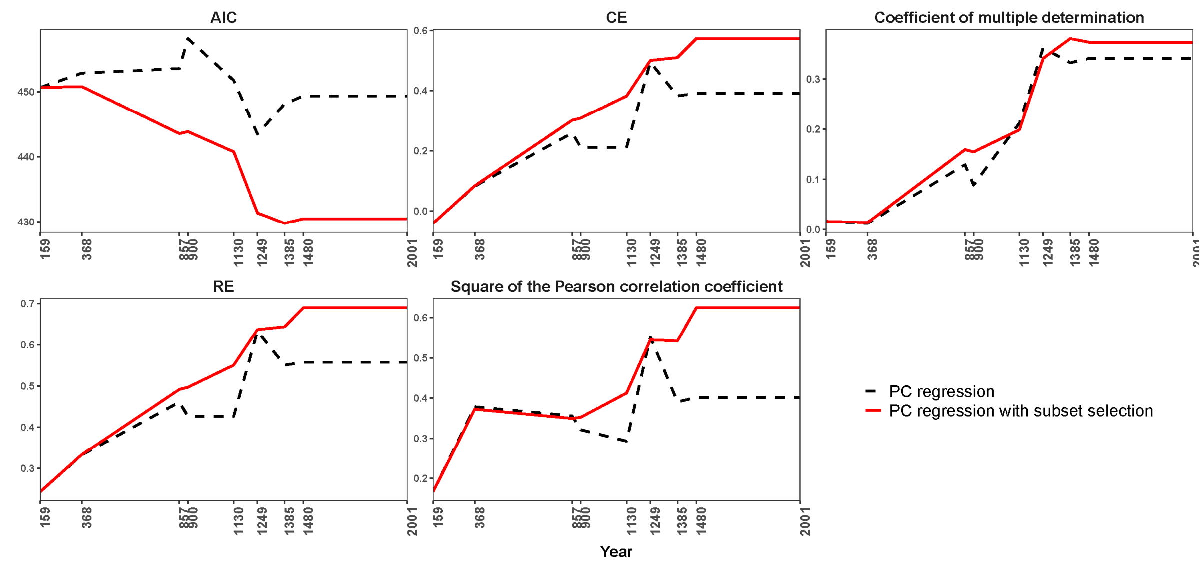

Figure 5. Line graph of the variability of AIC, $CRSQ$, $VRSQ$, CE, and RE values for nests as the number of predictors increases

Figure 6 shows the reconstructed streamflow and instrumental streamflow during the test period. Although the reconstructed series is lower than the instrumental record on most individual years, it estimates low flows, long-term trends and evolution feature well.

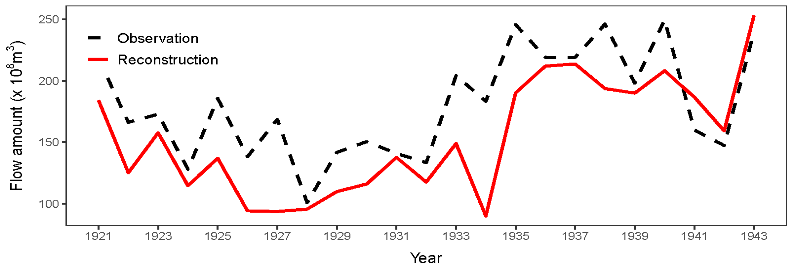

Figure 6. The instrumental streamflow series and the reconstructed streamflow series during the overlap time of 1921-2002. The dotted line divides the calibration period and the validation period.

4.2 HCYRB streamflow reconstruction and evolution analysis

The annual streamflow of HCYRB at Tangnaihai Station was reconstructed back to 159 C.E. The evolution characteristics of the streamflow were analyzed with statistical parameters as shown in Table 3. The results show that (1) the means of streamflow during 1400-1499 C.E., 700-799 C.E. are lower than 17 billion m^3; while the means of streamflow during 1500-1599 C.E and 500-599 C.E are respectively up to 21.13 billion $m^3$and 21.06 billion m^3; (2) the median values are usually smaller than mean values except for 1500-1599 C.E., 1400-1499 C.E., 1200-1299 C.E., 1000-1099 C.E., 700-799 C.E. and 159-199 C.E.; (3) the standard deviation of streamflow usually varies from 3 to 5 billion m^3 except 159-299 C.E., which is up to 5.34 billion m^3.

Table 3. The evolution characteristics of the annual streamflow of HCYRB.

Streamflow series		Mean (10^8 m^3)	Median (10^8 m^3)	Std. Dev. (10^8 m^3)
Instrumental series	1921-2016 C.E.	197.68	189.54	47.78
Reconstructed series	1800-1920 C.E.	193.56	193.36	45.77
	1700-1799 C.E.	174.45	170.67	44.96
	1600-1699 C.E.	187.69	183.15	48.61

Streamflow series	Mean (10^8 m^3)	Median (10^8 m^3)	Std. Dev. (10^8 m^3)
1500-1599 C.E.	211.32	216.79	43.78
1400-1499 C.E.	152.60	153.09	36.98
1300-1399 C.E.	201.95	201.54	46.47
1200-1299 C.E.	204.99	208.04	44.54
1100-1199 C.E.	175.73	172.06	49.99
1000-1099 C.E.	190.79	198.75	37.64
900-999 C.E.	186.70	185.07	46.74
800-899 C.E.	182.31	177.34	36.36
700-799 C.E.	164.43	165.56	36.92
600-699 C.E.	178.66	173.64	34.42
500-599 C.E.	210.63	208.21	36.09
400-499 C.E.	180.51	175.74	39.77
300-399 C.E.	202.32	203.30	48.58
200-299 C.E.	192.37	187.99	53.43
159-199 C.E.	201.40	204.63	51.52

Figure 7 shows the reconstructed streamflow time series (159-1920 C.E.) adjoined with the instrumental streamflow time series (1921-2016 C.E.). The reconstruction results show that (1) the maximum annual streamflow is 33.08 billion m^3 in 198 C.E., while the minimum one is 6.50 billion m^3 in 908 C.E.; (2) the annual streamflow exhibits a skewed distribution of more dry years and fewer rainy years in a period.

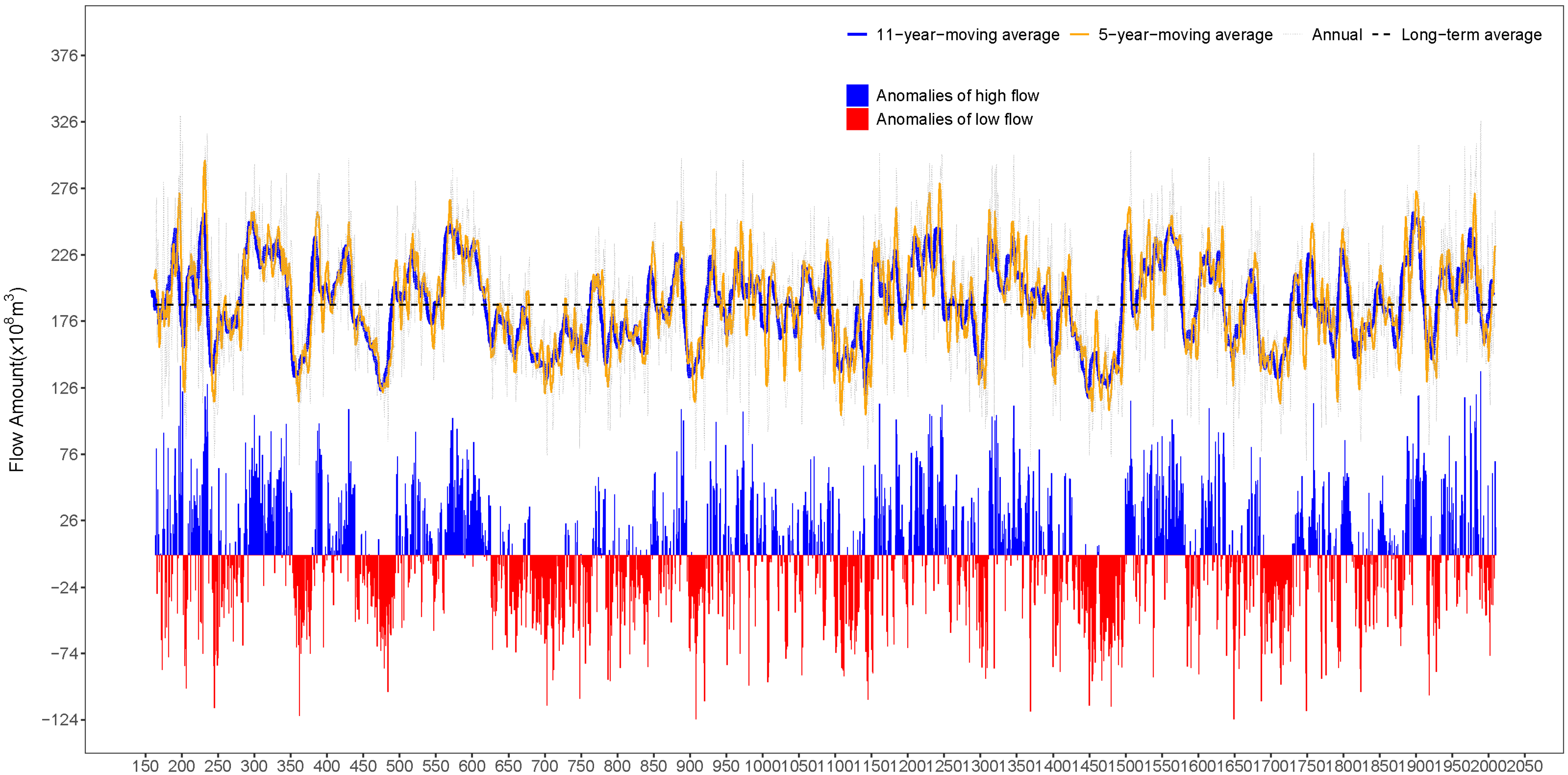

Figure 7. The adjoined streamflow of reconstruction and observation (grey line) at Tangnaihai Station over the time of 159 C.E. to 2016 C.E. along with the 5-year-moving average (yellow line), 11-year-moving average (green line). Blue vertical lines represent anomalies of high flow and red vertical lines represent anomalies of low flow.

4.3 Variability of high-flow and low-flow periods at HCYRB

The variability of high and flow periods in the last nearly two millennia is shown in Figure 8. The high flow periods are illustrated with blue vertical bars and low ones are illustrated with red vertical bars in the figure. The significant high and flow periods were highlighted in yellow and purple circles respectively which were discussed in next section. The low flow period divider of the 67th percentile of long-term streamflow is 16.563 billion m^3 and the high flow period divider of the 33rd percentile is 20.84 billion m^3.

As Figure 8 shows, 131 high flow periods incurred in the last nearly two millennia. During the last nearly two millennia (159-2016 C.E.), the high flow with the largest magnitude of 61.22 billion m^3 incurred between 293 C.E. and 307 C.E.; the longest high flow happened during 1569 C.E, and 1579 C.E. with a duration of 16 years; the most severe high flow happened during 1975 C.E. to 1976 C.E. with the severity of 8.23 billion m^3/year. In terms of duration, HCYRB incurred the 15- year high-flow period during 293-307 C.E., the 11-year high-flow period during 602-612 C.E and 1896-1906 C.E.., the 10- year high-flow period during 318-327 C.E., besides the 16-year one. In terms of severity, HCYRB incurred severe high-flow periods in 9196-201 C.E. (6.61 billion m^3/year), 230-236 C.E. (8.04 billion m^3/year), 888-889 C.E. (6.47 billion m^3/year), 1320-1322 C.E. (7.09 billion m^3/year) besides the most severe one.

Figure 8 shows that 136 low flow periods happened in the last nearly two millennia. During the last nearly two millennia (159-2016 C.E.), the low flow with the largest magnitude of 81.49 billion m^3 incurred between 1464 C.E. and 1485 C.E.; the longest low flow with a duration of 22 years incurred during 1464-1485 C.E and 1464-1485 C.E.; the most severe low flow happened during 1748 C.E. to 1749 C.E. with the severity of 8.04 billion m^3/year. In terms of duration, HCYRB incurred long low-flow periods during 903-914

C.E.(12 years), 1446-1459 C.E.(14 years), 1697-1707 C.E.(11 years) and 1709-1719 C.E.(11 years), besides the 22-year one. In terms of severity, HCYRB incurred severe low flows in 91368-1369 C.E. (6.76 billion m^3/year), 1648-1649 C.E. (6.73 billion m^3/year), 1775-1776 C.E. (5.61 billion m^3/year) besides the most severe one.

In general, the durations and magnitudes of low-flow periods are longer and larger than high-flow periods and the severities of high-flow periods are greater than low-flow periods. The most severe low flow is 0.19 billion m^3/year less than the most severe high flow, while the longest low-flow period is 6 years longer than the longest high-flow period and the magnitude of the largest low flow is 20.27 billion m^3 larger than that of the largest high flow The most severe 3 high-flow periods exhibited severities greater than 7.0 billion m^3/year, while only the most severe low-flow period exhibited severities greater than the value.

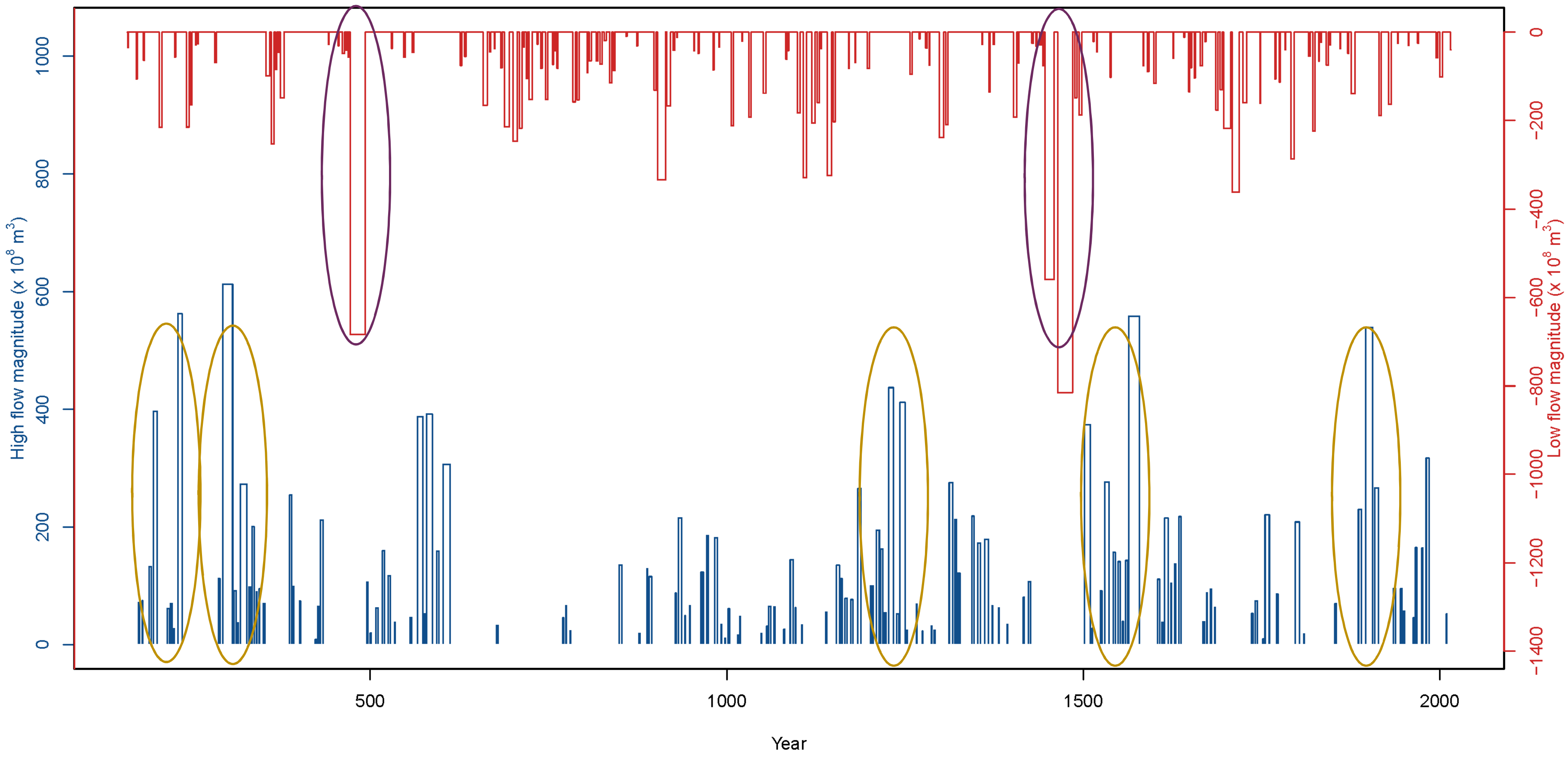

Figure 8. The magnitude and duration of low-flow periods (red vertical bar) and high-flow periods (blue vertical bar) over the period of 159 C.E. to 2016 C.E (The significant high-flow and low-flow periods were marked with yellow and purple circles respectively)

5 Discussion

A tree-ring-based reconstruction of annual streamflow for the past 1858 years, which is much longer than existing reconstruction, was developed for the headwater catchment of the Yellow River basin. The significant high-flow periods of the basin during the last two millennia are the early 3rd century, circa 300 C.E., early 13th century, 16th century and circa 1900 C.E. as the yellow circles show in Figure 8. The periods of the early 3rd century, circa 300 C.E., early 13th century and circa 1900 C.E correspond to the Roman Warm Period (the 1st century B.C. to the mid-4th century C.E), Medieval Warm Period (the mid-10th century to the end of the 13th century C.E) and Warming Period in the 20th century(Ge et al., 2013; Lamb, 1965). The high flow circa 1900 C.E also coincides with heavy precipitation in this period under a warm climate (Yang et al., 2014). Previous studies give the interpretation of a dominant moisture control on tree growth in this region and the monsoon precipitation is the main driven factor of the streamflow (Li et al., 2008; Qin et al., 2013; Yang et al., 2013). The phenomenon is likely caused by the increasing solar radiation in the Medieval Warm Period and Warming Period (Song et al., 2016; Yan Mi et al., 2014). The purple circles in Figure 8 show that the most significant low-flow periods of the basin during the last two millennia are the late 5th century and late 15th century, which corresponds to the Dark Age Cold Period (the end of the 4th century to the early of 10th century C.E) and Little Ice Age Period (the 15th to 19th century). The late-15th-century low flow coincides with historical archives of droughts in Beijing, Shandong, Shanxi, Henan, and Shannxi and is widely proved by the existing reconstructions by Wang et al. (2016b), Gou et al. (2007) and Gou et al. (2010). Existing research gives evidence that the low-flow period of the late 15th century in the headwater catchment of the Yellow River basin should be due to precipitation decrease caused by weak solar activity, which resulted in a thermal contrast between sea and land and weakened monsoons (Eddy, 1976; Gou et al., 2010). The reconstruction suggests that a warm climate is more likely accompanied by a high-flow period and low-flow periods are more likely to happen in cold periods associated with the Asian Summer Monsoon and solar activity (Han et al., 2019; Zheng et al., 2014).

6 Conclusion

This study presents a new annual (Nov-Oct) streamflow reconstruction at HCYRB back to 159 C.E. using 12 standard tree-ring chronologies. The new streamflow series was reconstructed in water year same with the cascade reservoir operation and provides useful information for water resources management of the basin. The nested reconstruction models with a combination of the nested principal component regression approach and the stepwise best tree-ring subset selection method were proposed. The results of the model assessment verify that the proposed model is capable of reconstructing annual streamflow accurately with strong model skills in terms of AIC, $CRSQ$, $VRSQ$, CE, and RE.

The high and low flow periods during the last two millennia were analyzed in terms of the magnitude, severity, and duration to further explore the history streamflow variation. In general, the significant high-flow periods are the early 3rd century (230-236 C.E.), circa 300 C.E. (293-307 C.E.), early 13th century (1227-1234 C.E. and 1243-1250C.E.), 16th century (1502-1510 C.E. and 1564-1579 C.E.) and circa 1900 C.E. (1896-1906 C.E.), while the low-flow periods are the late 5th century (472-493 C.E.) and late 15th century (1446-1459 C.E. and 1464-1485 C.E.). The reconstruction suggests that a warm climate is more likely accompanied by a high-flow period and low-flow periods are more likely to occur in cold periods associated with the Asian Summer Monsoon and solar activity.

The new approach can be applied to other areas, which improves the reconstruction accuracy and enriches the model library. The new reconstruction extends streamflow data of HCYRB from just 100 years of observations to 1,858 years including 131 high flow periods and 136 low flow periods, which provides adequate data foundation to analyze periodic variation and succession characteristics of streamflow. The analyses of significant high-flow and low-flow periods show the historical condition and give evidence of the mechanisms by which climate drives streamflow. Consequently, the results give further information to streamflow prediction of HCYRB and long-term optimal operation of Longyangxia over-year regulation reservoir.

Acknowledgments, Samples, and Data

Streamflow data are from the Yellow River Conservancy Commission of the Ministry of Water Resources at HydroShare, http://www.hydroshare.org/resource/bde8bcf096544ce7b183de784a378c52. The tree ring data are downloaded from the International Tree-Ring Data Bank (ITRDB) (https://www.ncdc.noaa.gov/data-access/paleoclimatology-data/datasets/tree-ring). The project was financially supported by the National Natural Science Foundation of China (Grant No. 52109010), the Postdoctoral Science Foundation of China (2021M701047), the Fundamental Research Funds for the Central Universities (B210202012) and the National Key Research and Development Program of China (Grant No. 2018YFC1508200). Rao acknowledges funding from the National Science Foundation Office of Polar Programs (NSF-OPP) Arctic Social Sciences grant #1737788 and the NOAA Climate and Global Change Postdoctoral Fellowship Program, administered by UCAR’s Cooperative Programs for the Advancement of Earth System Science (CPAESS) under award # NA18NWS4620043B."

References:

Ahmed, M. et al., 2013. Continental-scale temperature variability during the past two millennia. Nature geoscience, 6(5): 339.

Ammann, C.M., Genton, M.G., Li, B., 2010. Technical Note: Correcting for signal attenuation from noisy proxy data in climate reconstructions. Clim. Past, 6(2): 273-279. DOI:10.5194/cp-6-273-2010

Burnham, K.P., Anderson, D.R., 2004. Multimodel Inference Understanding AIC and BIC in Model Selection. Sociological Methods & Research, 33(33): 261-304.

Cook, E.R., 1985. A TIME SERIES ANALYSIS APPROACH TO TREE RING STANDARDIZATION (DENDROCHRONOLOGY, FORESTRY, DENDROCLIMATOLOGY, AUTOREGRESSIVE PROCESS).

Cook, E.R., Briffa, K.R., Jones, P.D., 1994. Spatial regression methods in dendroclimatology: a review and comparison of two techniques. International Journal of Climatology, 14(4): 379-402.

Cook, E.R. et al., 2013. Five centuries of Upper Indus River flow from tree rings. Journal of hydrology, 486: 365-375.

Devineni, N., Lall, U., Pederson, N., Cook, E., 2013. A tree-ring-based reconstruction of Delaware River basin streamflow using hierarchical Bayesian regression. Journal of Climate, 26(12): 4357-4374.

Eddy, J.A., 1976. The Maunder Minimum. ence, 192(192): 1189-1202.

Emile-Geay, J. et al., 2017. A global multiproxy database for temperature reconstructions of the Common Era. Scientific data, 4: 170088.

Fritts, H., 1976. Tree rings and climate, 567 pp. Academic, San Diego, Calif.

Fritts, H.C., 1991. Reconstructing large-scale climatic patterns from tree-ring data: t diagnostic analysis. University of Arizona Press.

Gaire, N.P. et al., 2017. Tree-ring based spring precipitation reconstruction in western Nepal Himalaya since AD 1840. Dendrochronologia, 42: 21-30.

Ge, Q., Zheng, J., Hao, Z., Liu, H., 2013. General characteristics of climate changes during the past 2000 years in China. Science China Earth Sciences, 56(2): 321-329. DOI:10.1007/s11430-012-4370-y

Gou, X. et al., 2007. Streamflow variations of the Yellow River over the past 593 years in western China reconstructed from tree rings. Water Resources Research, 43(6).

Gou, X. et al., 2010. Tree ring based streamflow reconstruction for the Upper Yellow River over the past 1234 years. Chinese Science Bulletin, 55(36): 4179-4186.

Han, J., Yang, Y., Man, Z., 2019. Reconstruction and analysis of sequence of extreme drought events in north of China during AD 1000-2000. Journal of Palaeogeography, 21(4): 675-684. DOI:10.7605/gdlxb.2019.04.045

Helama, S., Lindholm, M., Timonen, M., Eronen, M., 2004. Detection of climate signal in dendrochronological data analysis: a comparison of tree-ring standardization methods. Theoretical and Applied Climatology, 79(3-4): 239-254.

Hidalgo, H.G., Piechota, T.C., Dracup, J.A., 2000. Alternative principal components regression procedures for dendrohydrologic reconstructions. Water Resources Research, 36(11): 3241-3249.

Huang, S., Chang, J., Leng, G., Huang, Q., 2015. Integrated index for drought assessment based on variable fuzzy set theory: a case study in the Yellow River basin, China. Journal of Hydrology, 527: 608-618.

Keyimu, M. et al., 2020. Tree ring–based minimum temperature reconstruction in the central Hengduan Mountains, China. Theoretical and Applied Climatology, 141(1): 359-370. DOI:10.1007/s00704-020-03169-5

Lamb, H.H., 1965. The early medieval warm epoch and its sequel. Palaeogeography, Palaeoclimatology, Palaeoecology, 1: 13-37. DOI:https://doi.org/10.1016/0031-0182(65)90004-0

Li, J. et al., 2008. Common tree growth anomalies over the northeastern Tibetan Plateau during the last six centuries: implications for regional moisture change. Glob. Change Biol., 14(9): 2096-2107. DOI:10.1111/j.1365-2486.2008.01603.x

Li, Q., Yang, M., Wan, G., Wang, X., 2016. Spatial and temporal precipitation variability in the source region of the Yellow River. Environmental earth sciences, 75(7): 594.1-594.14.

Margolis, E.Q., Meko, D.M., Touchan, R., 2011. A tree-ring reconstruction of streamflow in the Santa Fe River, New Mexico. Journal of Hydrology, 397(1-2): 118-127.

Meko, D., Stockton, C.W., Boggess, W.R., 1995. THE TREE-RING RECORD OF SEVERE

SUSTAINED DROUGHT 1. JAWRA Journal of the American Water Resources Association, 31(5): 789-801.

Meko, D.M., Therrell, M.D., Baisan, C.H., Hughes, M.K., 2001. SACRAMENTO RIVER FLOW RECONSTRUCTED TO AD 869 FROM TREE RINGS 1. JAWRA Journal of the American Water Resources Association, 37(4): 1029-1039.

Meko, D.M. et al., 2007. Medieval drought in the upper Colorado River Basin. Geophysical Research Letters, 34(10).

Melvin, T.M., Briffa, K.R., 2008. A “signal-free” approach to dendroclimatic standardisation. Dendrochronologia, 26(2): 71-86. DOI:https://doi.org/10.1016/j.dendro.2007.12.001

Melvin, T.M., Briffa, K.R., Nicolussi, K., Grabner, M., 2007. Time-varying-response smoothing. Dendrochronologia, 25(1): 65-69. DOI:10.1016/j.dendro.2007.01.004

Michaelsen, J., 1987. Cross-validation in statistical climate forecast models. Journal of climate and Applied Meteorology, 26(11): 1589-1600.

Qin, C. et al., 2013. Radial Growth of Qilian Juniper on the Northeast Tibetan Plateau and Potential Climate Associations. Plos One.

Rao, M.P. et al., 2018. Six centuries of Upper Indus Basin streamflow variability and its climatic drivers. Water Resources Research.

Schwarz, G., 1978. Estimating the dimension of a model. The annals of statistics, 6(2): 461-464.

Shiau, J.T., Feng, S., Nadarajah, S., 2007. Assessment of hydrological droughts for the Yellow River, China, using copulas. Hydrological Processes: An International Journal, 21(16): 2157-2163.

Smith, L.P., Stockton, C.W., 1981. Reconstructed Stream Flow for the Salt and Verde Rivers From Tree-Ring Data 1. JAWRA Journal of the American Water Resources Association, 17(6): 939-947.

Song, Y. et al., 2016. Analysis on Interdecadal Correlation between Solar Activity and Snow Depth over the Qinghai-Xizang Plateau and East Asian Atmospheric Circulation in Winter. Plateau Meteorology.

Stockton, C.W., Jacoby, G.C., 1976. Long-term surface-water supply and streamflow trends in the Upper Colorado River basin based on tree-ring analyses, 18. Lake Powell Res Proj Bull, 1-70 pp.

Timilsena, J., Piechota, T., Tootle, G., Singh, A., 2009. Associations of interdecadal/interannual climate variability and long-term colorado river basin streamflow. Journal of Hydrology, 365(3-4): 289-301.

Timilsena, J., Piechota, T.C., Hidalgo, H., Tootle, G., 2007. Five Hundred Years of Hydrological Drought in the Upper Colorado River Basin 1. JAWRA Journal of the American Water Resources Association, 43(3): 798-812.

Wang, F., Wang, Z., Yang, H., Zhao, Y., 2018a. Study of the temporal and spatial patterns of drought in the Yellow River basin based on SPEI. Science China Earth Sciences: 1-14.

Wang, T. et al., 2018b. Historical and future changes of frozen ground in the upper Yellow River Basin. Global and Planetary Change, 162: 199-211. DOI:https://doi.org/10.1016/j.gloplacha.2018.01.009

Wang, Y., Wang, W., Peng, S., Jiang, G., Wu, J., 2016a. The relationship between irrigation water demand and drought in the Yellow River basin. Proceedings of the International Association of Hydrological Sciences, 374: 129-136.

Wang, Y., Wang, W.H., Peng, S.M., Jiang, G.Q., Wu, J., 2016b. The relationship between irrigation water demand and drought in the Yellow River basin, International Conference on Water Resources Assessment and Seasonal Prediction. Copernicus Gesellschaft Mbh, German Fed Inst Hydrol, Koblenz, GERMANY, pp. 129-136. DOI:10.5194/piahs-374-129-2016

Woodhouse, C.A., Lukas, J.J., 2006. Multi-century tree-ring reconstructions of Colorado streamflow for water resource planning. Climatic Change, 78(2-4): 293-315.

Yan Mi, Wang Zhiyuan, Jian, L., 2014. Simulation of the characteristics and mechanisms of Chinese typical warm periods over the past 1500 years. Quaternary Sciences, 34(6): 1166-1175. DOI:10.3969/j.issn.1001-7410.2014.06.05

Yang, B., He, M., Melvin, T.M., Zhao, Y., Briffa, K.R., 2013. Climate Control on Tree Growth at the Upper and Lower Treelines: A Case Study in the Qilian Mountains, Tibetan Plateau. PLOS ONE, 2013,8(7) AR e69065(-): -.

Yang, B. et al., 2014. A 3,500-year tree-ring record of annual precipitation on the northeastern Tibetan Plateau. Proc. Natl. Acad. Sci. U. S. A., 111(8): 2903-2908. DOI:10.1073/pnas.1319238111

Yin, J. et al., 2021. Does the Hook Structure Constrain Future Flood Intensification Under Anthropogenic Climate Warming? Water Resources Research, 57(2): e2020WR028491. DOI:10.1029/2020WR028491

Zhang, W. et al., 2014. Spatiotemporal Change of Blue Water and Green Water Resources in the Headwater of Yellow River Basin, China. Water Resources Management, 28(13): 4715-4732. DOI:10.1007/s11269-014-0769-x

Zhang, Y., Li, F., Peng, S., Li, K., 2019. Study on the Joint Operation of Key Reservoirs to Cope with Drought in the Yellow River Main Stream. Yellow River.

Zhang, Y. et al., 2015. Impact of projected climate change on the hydrology in the headwaters of the Yellow River basin. Hydrological Processes, 29(20): 4379-4397.

Zheng, J. et al., 2014. Changing characteristics of extreme climate events during past 2000 years in China. Progress in Geography, 33(1): 3-12.

Zheng, Y., Huang, Y., Zhou, S., Wang, K., Wang, G., 2018. Effect partition of climate and catchment changes on runoff variation at the headwater region of the Yellow River based on the Budyko complementary relationship. Science of The Total Environment, 643: 1166-1177.